



**ARTICLE**

# Effects of Cationic Surfactant on Fresh and Hardened Properties of Cement-Based Mortar

Soumaya Zormati, Fadhel Aloulou\* and Habib Sammouda

Laboratory of Energy and Materials, LabEM-LR11ES34, University of Sousse, Sousse, Tunisia

\*Corresponding Author: Fadhel Aloulou. Email: alouloufadhel@gmail.com

Received: 21 August 2022 Accepted: 20 October 2022

## ABSTRACT

The objective of this study is to analyze the effects of using surfactant (CTAB) and cellulose nanofibers (NFC) as an admixture in cement mortars. We examined composite properties as porosity, compression energy, thermal conductivity and hydration. The results showed that with the addition of 0.7% by weight of NFC per emulsion in the presence of a cationic surfactant (CTAB). The new material produced presented a dry porosity between 4.7% and 4.4%, compressive strength between 9.8 and 22.9 MPa, and thermal conductivity between 0.95 and 2.25  $W \cdot m^{-1} \cdot K^{-1}$ . Thus we show better mechanical and thermal performance than that traditional Portland cement mortar with a density similar. In addition, the mortar made by emulsion of ordinary portland cement, cellulose nanofiber and organophilic clay (OC) treated with cetyltrimethylammonium bromide (CTAB) obtained has good resistance under high temperature and water, as well as excellent thermal insulation performance under high temperature and humidity conditions. This study verified that the presence of NFC promotes hydration, leading to the production of more calcium silicate and portlandite gel.

## KEYWORDS

Cement; nanofiber cellulose; organophile-clay; thermal conductivity; hydration; surfactant; compressive strength; mortar

## Nomenclature

CTAB	Cetyltrimethylammonium Bromide
C-S-H	Calcium-Silica-Hydration
NaOH	Sodium Hydroxide
OPC	Ordinary Portland Cement
OC	Organophilic Clay
NFC	Nanofiber Cellulose
TEMPO	2,2,6,6-Tetramethylpiperidine 1-oxyl, 2,2,6,6-tetramethyl-1-piperidinyloxy
NaBr	Sodium Bromide

## 1 Introduction

In Tunisia, several agricultural wastes have been used in research on composite cement as a building fiber with building and construction materials, including wood, palm fiber, *Posidonia oceanica* and Alfa



[1]. Indeed, there are many benefits to using fibers made from biological sources, including their wide availability, low cost, large specific surface area and unique mechanical qualities [2]. When natural vegetable fibers are added to concrete during the mixing process, the characteristics of simple concretes are improved. These fibers have long been utilized to reinforce clay and mud. On the mechanical characteristics, structural behavior, and potential applications of natural fibers in buildings, numerous studies have been published.

Currently, a variety of cementitious composites based on clay minerals and natural fibers are utilized in a variety of applications, including the building industry. Materials made of natural clay in particular offer strong thermal insulation qualities, low mechanical resistance and nevertheless [3]. However, various techniques were developed to enhance the physicochemical characteristics of the wood fibers using clay and cement [4]. Nanofiber cellulose is now used for a variety of applications, including acoustic protection, thermal insulation, environmental cleanup, aviation, and bio medicine [5].

For reasons of high energy consumption, it is necessary to look for new materials to store energy and conserve it. Current research has focused on the creation of insulating building materials, with excellent mechanical and thermal properties. But the improvement of mechanical residences leads to a general lack of thermal insulation performance. The majority of general electricity consumed in homes these days is used for heating and cooling [6].

To maintain thermal comfort within buildings, it is mandatory to use materials with high heat exchange performance with phase change materials in the building envelope. In this context, several studies consider the reasoning that adding thermal insulation materials to walls and roofs can improve energy consumption [7]. In the case of thermal insulation, these materials react as a substance that slows down the movement of heat into and out of building structures. One of the most important properties to look for in this study is thermal conductivity [8–10].

Nowadays, research on bio-composite materials, natural clay, vegetable fibers, sisal, flax, and wood fibers are used to reinforce the cementitious matrix to improve the mechanical properties, accelerate the production of calcium silicates, promote the hydration [11–13] and optimize the acoustic and thermal properties of composite materials based on a cementitious matrix [14,15]. Based on porous structures, suspensions of volcanic ash and natural clay particles have been the subject of several studies [16,17]. Given these properties and in this context, the case of clay composite materials was chosen for our study. Because of their abundance, availability and surface properties, exposed clays, modified or exchanged with polyelectrolytes, are used as filler or reinforcement in composite materials to improve the structural properties of cement-based composite materials [18]. In addition, it should be noted in many studies that the use of organophilic clay treated with a cationic surfactant, has attracted considerable importance in industrial research [19] due to its excellent performance in physico-chemical properties which possess (high specific surface) [20].

It should be noted that the developments in the sectors of buildings and green building materials, biodegradable and environmentally friendly, have approved that the use of natural fibers contributes to minimizing the release of CO<sub>2</sub> into the atmosphere [21]. Cellulose nanofibers offer many advantages, but they also have several disadvantages that have limited their use outside the building and cementitious composite materials sectors. Indeed, the interfacial adhesion that initially exists between the fibers and the cementitious matrix is relatively low, and the mechanical characteristics and their durability are negatively affected by the degradation of the fibers in the cementitious matrix [22]. In addition, the addition of clay to a cementitious matrix is limited, which poses problems in their use.

In order to improve the mechanical and thermal properties and reduce the alkalinity rate of the cementitious matrix, we have reduced and blocked the formation of Ca(OH)<sub>2</sub>, through the use of cement-based composite materials that have been produced by incorporating cellulose nanofibers and

organophilic clay particles, while wishing to improve the microstructural properties and the reinforcing properties between the matrix and the cellulose nanofibers [23,24]. To achieve this objective, it is interesting to use the CTAB surfactant as an adjuvant between the cellulose nanofiber (NFC) and the treated organophilic clay platelets in order to promote the interaction with  $\text{Ca}(\text{OH})_2$  by producing a gel of calcium-silica (C-S-H) hydration. The Zeta potential has been used to describe the charge on the surface of cellulose nanofibers (NFC). In addition, X-ray diffraction, FTIR and SEM were used to characterize organic clay in powder form. Mechanical treatment of the clay with cetyltrimethylammonium bromide (CTAB) produced the organic clay. The physical characteristics and thermal conductivity of cement composites reinforced with cellulose nanofibers are researched and analyzed.

## 2 Materials and Methods

### 2.1 Materials

Quaternary alkyl ammonium salt CTAB (Mw 336.39 g/mol) is a cationic surfactant that is soluble in water and is used to make OC.

For cementitious matrix composites, CTAB-modified cellulose nanofibers (NFC) and organophilic clay (OC) have been employed as reinforcement. This organophilic clay is a natural clay treated with a cationic surfactant CTAB. All the mortars developed are based on a cementitious matrix. The cement used in our work is Ordinary Portland Cement: OPC (NFP15-301) (Table 1).

**Table 1:** Chemical composition of Ordinary Portland Cement [25,26], Copyright © 2019, Tech Science Press

Oxides	Cement (wt%)
CaO	65.47
SiO <sub>2</sub>	19.82
Al <sub>2</sub> O <sub>3</sub>	4.66
Fe <sub>2</sub> O <sub>3</sub>	3.03
MgO	0.84
K <sub>2</sub> O	0.64
Na <sub>2</sub> O	0.10
TiO <sub>2</sub>	0.16
SO <sub>3</sub>	2.87
Loss ignition (LOI)	3.50
Density	3.2 g/cm <sup>3</sup>
Specific surface area	355 m <sup>2</sup> /Kg
Average particle size	18.54 μm

### 2.2 Particle Size Determination

The particle size diameters of sand and their hydrodynamic diameters were measured at 20°C using a Malvern Nano-zetasizer ZS (Malvern, UK) with a fixed scattering angle of 173°. The dispersions were not diluted before starting the measurements [12]. Dynamic light scattering measurements gave a Z-average size that was used for the comparison of the different particles (Fig. 1).

Fig. 1 shows that the average volume of silica powder milled for 2 h was  $73.53 \cdot 10^{-6}$  m. The specific surface of quartz sand was  $0.83 \text{ m}^2 \cdot \text{g}^{-1}$ .

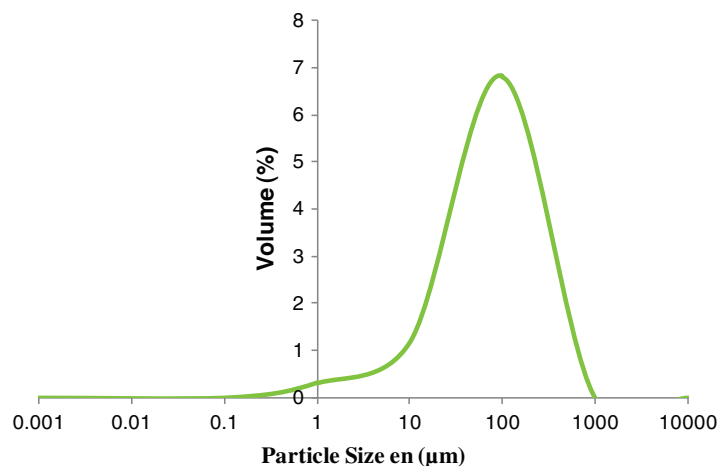


**Figure 1:** Particle size distribution of silica sand

### 2.3 The Process of Making Organophilic-Clay (OC)

The clay was prepared to be modified with CTAB for 3 h in order to establish the amorphous phase of the treated clay. In order to synthesize organophilic clays [27], 10 ml of hydrochloric acid [1M] must be added. Then, the acid solution's temperature is increased to 80°C. Once this temperature has stabilized,  $10^{-2}$  moles of CTAB are added. After four hours of stirring and cationic exchange at 80°C, 10 g of clay is added. The inorganic cations are subsequently removed by filtering and reintroducing the clay. The clay is properly cleaned before being dried in an oven at 80°C. It has been shown in numerous experiments that the intercalation of CTAB cationic surfactants with clay, not only modifies the hydrophilic characteristics of the clay surface, but also the space between the clay layers, giving rise to a very porous clay.

### 2.4 The Processing Process of Cellulose Nanofibers

Using a high-pressure homogenizer (NS1001L PANDA 2K-GEA), we created nanofiber cellulose (NFC) from bleached eucalyptus pulp in accordance with methods previously described by our works [28]. In a nutshell,  $500 \times 10^{-6}$  mol/g of oxidation was initially applied to the bleached cellulose fibers [26]. Then, fibrillation was performed by running the fiber suspension (2% by weight) through the homogenizer ten times at a pressure of 600 bar.

### 2.5 Mix Proportions

A mortar of cement-based composite materials cement with a water-cement ratio (w/c) of 0.6 was applied for all the mixtures according to the Tunisian standard NT 47.05 [16]. Before blending, the cement and organophilic clay were first dry-blended for five minutes at a low speed. A mass ratio of 0.6 percent water to cement was used to prepare each sample. The cement pastes were mixed in a mixer specified according to NT 47.05 [16], and the cement mortar composites reinforced with nanofibrillated cellulose were prepared with 0% NFC, 0.1%, 0.3%, 0.5%, 0.7%, 1%, 1.5%, and 2% by weight of cement (Table 2).

For compressive strength testing, cylindrical specimen samples with a cross section of 3.5 mm and a height of 7 mm were made using various mixtures. The compressive strength results are the average of the three test values (Table 3).

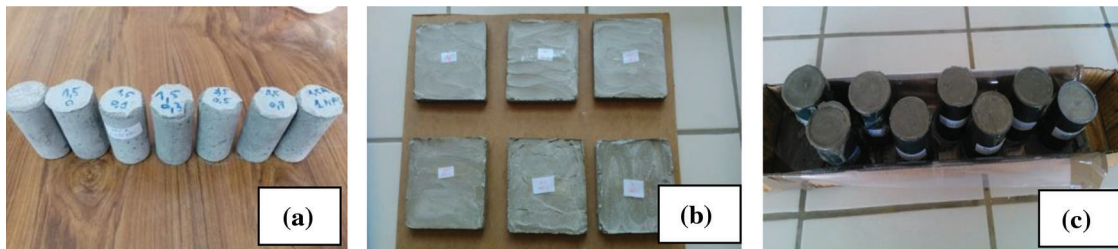
The samples were taken out of the mold after 24 h and hardened to a relative humidity of 95% and a temperature of roughly 25.0°C (Fig. 2). Compressive strength tests were performed in accordance with NT 47.05 requirements after 1, 7, and 28 days of hardening [26].

**Table 2:** Mixture formulations

Samples	Compositions	Cement (g)	Sand (g)	Mass rate of NFC (%)	Mass rate of organophile clay (%)	W/C
NFC-0	Cement+sand	45	90	0	1	0.6
NFC-1	Cement+sand+NFC	45	90	0.1	1	0.6
NFC-2		45	90	0.3	1	0.6
NFC-3		45	90	0.5	1	0.6
NFC-4		45	90	0.7	1	0.6
NFC-5		45	90	1	1	0.6
NFC-6		45	90	1.5	1	0.6
NFC-7		45	90	2	1	0.6

**Table 3:** Shapes and dimensions of the prepared specimens

Shapes	Dimensions	Type of use
Cylindrical blocks	$\Phi = 35$ mm h = 70 mm	Compressive strength measurements
Boards	L = 100 mm w = 100 mm e = 10 mm	Thermal conductivity and contact angle measurements
Cylindrical pellets	$\Phi = 10$ mm h = 5 mm	Contact angle measurements

**Figure 2:** Shapes of (a) cylindrical, (b) boards and (c) pellets specimens

## 2.6 Testing and Curing

In order to conduct the mechanical tests, three series of specimens with dimensions (3.5 cm × 7 cm × 1.75 cm) were created. Following 24 h of casting, all specimens were removed from molds and submerged for roughly 1, 7, and 28 days. On an “MTS Insight” materials testing machine, tests for compressive strength were conducted.

## 2.7 Amount of Cement Hydration

By calculating the volume of non-evaporable water present in the cement pastes, the level of cement hydration was determined. After stopping hydration with acetone and drying to constant mass at 140°C, cement paste powders made from ground test prisms were analyzed. The samples were then heated to 1100°C and maintained there for 3 h. The samples are then held at room temperature until they cool before being put into a desiccator. The mass loss between 140°C and 1100°C, normalized by the flaming mass, was used to calculate the non-evaporable water content of the prepared samples [27].

## **2.8 Evaluation of Composite Materials Characteristics**

### **2.8.1 Zeta Potential**

Measurements of the electrophoretic mobility of the cellulose nanofibers in the aqueous suspension were made using a potential analyzer (Malven 2000). The fine fraction that was left after filtering the initial fiber suspension via a 45  $\mu\text{m}$  screen was used for the measurements. The potential values obtained by electrophoresis corresponded to the measurements of the potential made repeatedly across the whole suspension using the streaming potential technique (Mute kSZP06, using a 40  $\mu\text{m}$  screen as an electrode). Following four test measurements, the average of each potential value was calculated.

### **2.8.2 Infrared Fourier Transform Spectroscopy (FTIR)**

After being treated with NaOH, sulfuric acid, and/or CTAB, cellulose nanofiber and natural clay underwent functional group change analysis using Fourier Transform Infrared (FTIR) Spectroscopy. A Perkin Elmer FTIR spectrum was used for this test. The samples were measured with a resolution of 4  $\text{cm}^{-1}$  at room temperature. After baseline correction, all FTIR measurements were carried out in transmission mode.

### **2.8.3 X-Ray Diffraction (XRD)**

The XRD pattern was measured with an X-ray Diffractometer in the  $2\theta$  range between  $9^\circ$  and  $60^\circ$ , using  $\text{CuK}\alpha$  ( $\gamma = 1.54 \text{ \AA}$ ) radiation at 40 KV and 30 mA. With an exceptional analysis speed, with a step size of  $0.02^\circ/\text{s}$  a collection time of 40 s per step and an incident angle of  $1^\circ$ . The crystallization degree is obtained by comparing the intensity of the crystalline and the amorphous curve. The crystalline degree of organophile clay was calculated from an XRD profile. X-ray measurements were made on sample sheets pushed in powder after the air drying of the OC.

## **2.9 Thermal Conductivity**

22 cm  $\times$  22 cm  $\times$  1.5 cm samples were prepared and cured for 28 days to conduct thermal conductivity measurements using a "Heat Transmission Study Bench-PTC 100", the thermal conductivity of various samples with dimensions of 24.5 cm  $\times$  1.5 cm  $\times$  24.5 cm was tested.

The method of displacement with methanol was used to measure the porosity. After 28 days of hardening, the samples were ground into small particles. The particles ground after 28 days were cured and then vacuum dried to a constant weight of  $W_0$ . The dried particles were immersed in methanol for 24 h and the weight of the sample which contains the methanol was noted as  $W_1$ . Subsequently, the particles were extracted from the methanol and dried on the surface, and the measured weight was noted as  $W_2$ . The porosity of the samples was calculated as follows:  $P = (W_2 - W_0)/(W_2 - W_1)$ .

## **3 Results and Discussion**

### **3.1 The Time Setting**

The NFC-0.7 combination had the quickest setting times, as shown in Fig. 3, and both the initial and final setting times have dropped as NFC contents mixtures have decreased. The NFC-cement nanocomposites increased initial and final setting times varied from 6.1 to 38 and 1.8 to 23.38 percent, respectively. As a result, NFC can serve as an accelerator to cause hydration to happen more quickly.

### **3.2 Hydration Status**

Based on weight loss between  $140^\circ\text{C}$  and  $1100^\circ\text{C}$ , which is regarded as the amount of chemically bound water in the hardened cement pastes, the degree of cement hydration was determined [29]. The thermogravimetric measurement of the unhydrated cement revealed a mass loss at temperatures between  $600^\circ\text{C}$  and  $780^\circ\text{C}$ , which is consistent with calcium carbonate breakdown [29]. Calculating the mass of chemically bound water per unit gram of unhydrated cement by dividing the amount of chemically bound water by the final weight of the material yields the degree of hydration of the cement [30].

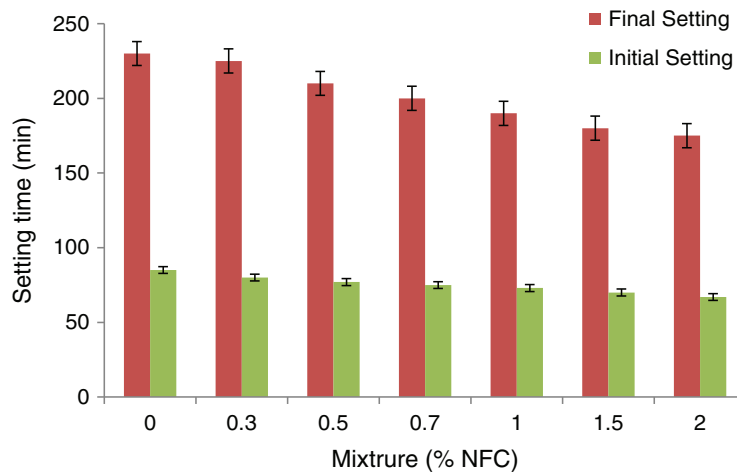


**Figure 3:** The settings times for NFC reinforcement pastes

Fig. 4 illustrates the evolution of the cement hydration level as a function of the NFC concentration at different hardening times. The level of cement hydration rises across the board for all cure ages as NFC cement paste content rises. The mixture containing 2 percent by weight of NFC results in the highest cement hydration value. After 1 and 28 days of hydration, respectively, the cement’s hydration rate is raised by 95% and 25% at this quantity of addition compared to the control mixture. NFC, on the other hand, increased early hydration in cement paste. In fact, after one day of curing, the cement’s degree of hydration increased by about 2 percent, 25 percent, 45 percent, 70 percent, 80 percent, 89 percent, and 95 percent for cement that contains 0% NFC and by weight, 0.3 percent, 0.5 percent, 0.7 percent, 1 percent, 1.5 percent, and 2 percent. Because NFC can have the same steric stabilizing effect as water-reducing admixtures, which guarantees uniform distribution of cement particles throughout the hydration process, the improvement in the degree of cement hydration was anticipated [31]. Additionally, NFC can serve as a nucleus to encourage the development of hydrated products, which will increase the cement early degree of hydration.

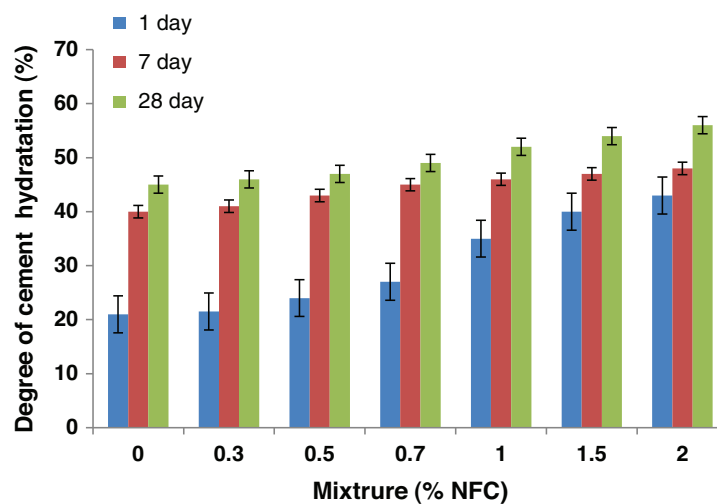


**Figure 4:** The evolution of cement hydration

### 3.3 X-Ray Diffraction-Based Mineralogical Characterization of the Hydration Products

XRD of cement with various NFC contents was conducted to determine how the addition of NFC is expected to impact the phase composition of cement. Fig. 5 displays similar diffraction patterns at a young stage of curing (one curing day). Portlandite, ettringite, and calcium silicate phases were among the predicted hydration products that were visible in the three samples' XRD patterns ( $C_3S$  and  $C_2S$ ). However, because the calcium silicate hydrates (C-S-H gel) are not well crystallized, it is difficult to distinguish the matching diffraction peaks in the patterns. As a result, the unreacted anhydrous cement phases are used to analyze the evolution of the C-S-H gel. With the addition of NFC, the calcium silicate major peaks become less intense because more anhydrous cement phases react in the presence of NFC ( $C_3S$  and  $C_2S$  are transformed into C-S-H). Additionally, compared to the control paste NFC 0 percent, larger concentrations of portlandite and ettringite are generated in the NFC 0.7 percent and NFC 1 percent samples. According to the amount of NFC added, the peak intensities change over time. By making more portlandite, ettringite, and C-S-H gel than the pure cement sample, it is discovered that the addition of NFC promotes the early hydration of the cement [32]. Contrarily, C-S-H, a binding phase of Portland cement that regulates the mechanical properties of cement, is one of the main hydration products. As a result, it can be said that the higher content of the C-S-H phase is likely the primary factor contributing to the significant improvement in the compressive strength of the cementitious matrix [33].

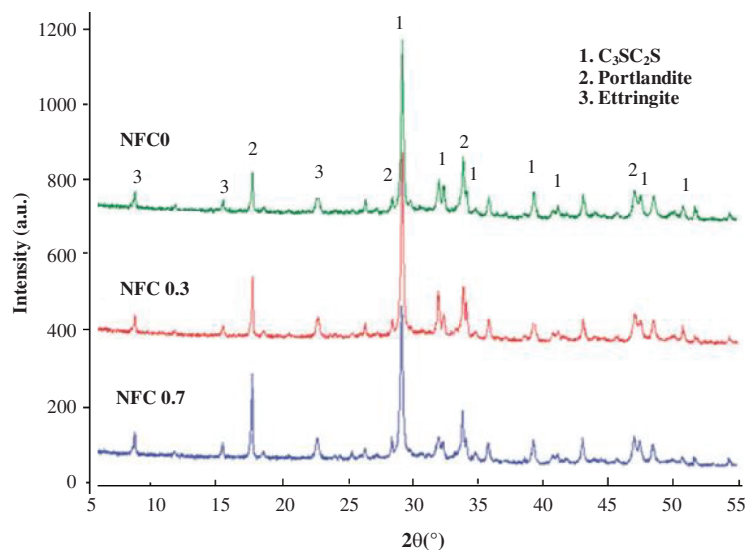


**Figure 5:** XRD spectrum of powder combinations containing (a) 0%, (b) 0.3%, and (c) 0.7% NFC

### 3.4 NFC and $Ca^{2+}$ Interaction in the Pore Solution

Additionally, as demonstrated in Fig. 6, complexity,  $COO^-$  can readily mix with  $Ca^{2+}$  in an interstitial solution. By cross-linking with two or four  $COO^-$  groups, a  $Ca^{2+}$  ion can cause the aggregation of these organic molecules [34,35]. This suggests that NFC with structure would aggregate as a result of combining with  $Ca^{2+}$  in a pore solution, as seen in Fig. 6.

NFC-containing  $COO^-$  groups can also react with  $Ca^{2+}$ , as illustrated in Fig. 6, and this reaction is probably due to electrostatic attraction rather than complexation. Furthermore, it can properly complete the first step of the interaction model by avoiding NFC agglomeration and benefiting from NFC disperse ion in the cement paste.

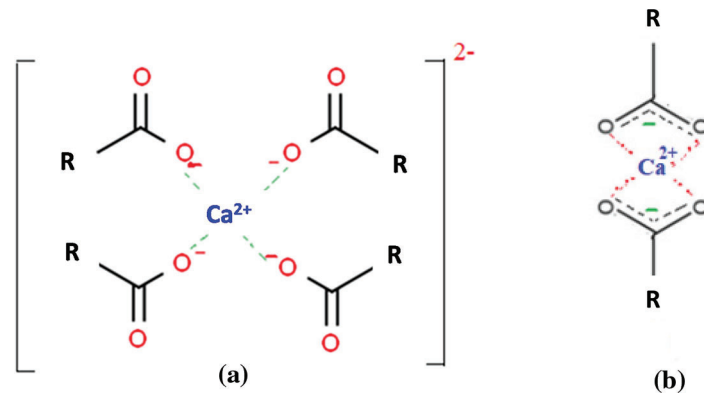


**Figure 6:** The complexity between  $\text{RCOO}^-$  and  $\text{Ca}^{2+}$

From the explanation above, it can be concluded that NFC particles have a lot of  $\text{COO}^-$  groups on their surfaces, and it is these surface groups that combine with  $\text{Ca}^{2+}$  to generate the adsorption of NFC and the rise in zeta potential (Fig. 7).

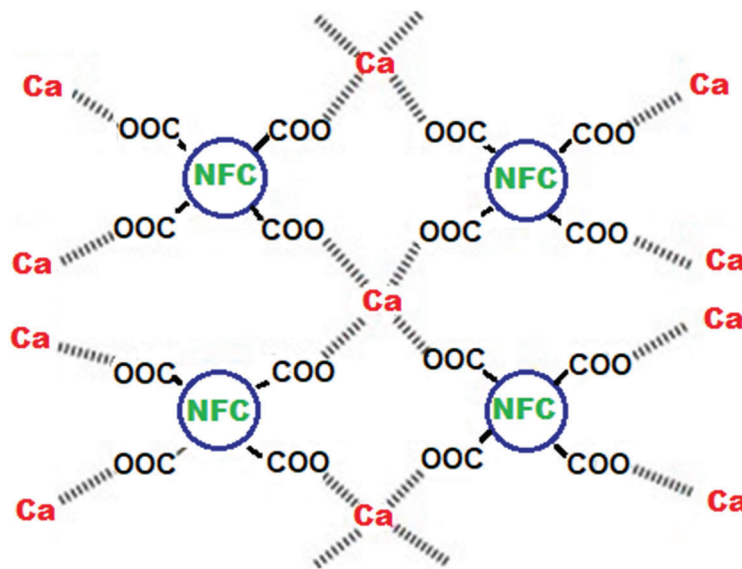


**Figure 7:** Reaction between  $(\text{NFC-COO}^-)$  and  $\text{Ca}^{2+}$  in solution

### 3.5 Potential Zeta

Fig. 8 shows that the zeta potential of the pure cement suspension was +5.5 mV. The rapid hydration of tricalcium aluminate (C3A) is mainly responsible for the existence of positive surface charges on cement grains [25,26]. However, the zeta potential is obviously decreased in the presence of the addition of NFC, which has negative surface charges because of the carboxylic groups produced during cellulose, delignification, and fiber discoloration [22]. With an addition of 0.30 percent, it becomes zero, whereas an addition of more than 0.30 percent results in a negative rise in the zeta potential. No zeta potential increase is visible for additions over 1.5 percent. In reality, the absolute value of zeta potential follows the same pattern of change with  $\text{Ca}^{2+}$  concentration by initially declining and then increasing. Given that large zeta potential causes increased surface adsorption, it may be inferred that the influence of NFC on the zeta potential may be one of the causes of the change in hydration. It is true that the following can

account for the shift in zeta potential. The negatively charged groups  $R-COO^-$  are to blame for the zeta potential of NFC, which is  $-33.5$  mV. The NFC can readily be adsorbed on the surface of the cement particles by electrostatic attraction because of its negative zeta potential. The positive zeta potential would be neutralized to zero as more NFC by mass % was added. Free  $Ca^{2+}$  ions can influence the environment of negatively charged cellulose nanofibers, resulting in increased or reduced repulsive forces between them, arguing that the presence of NFC promotes hydration, leading to the production of more calcium silicate and portlandite gel.

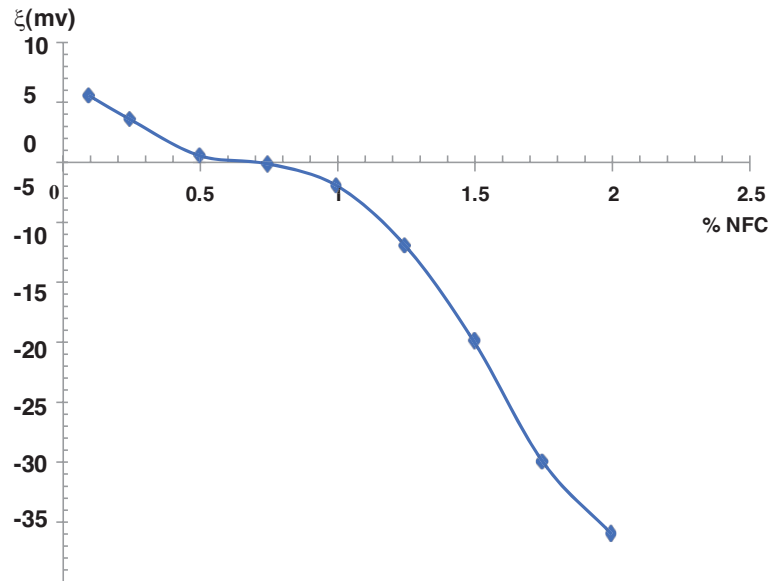


**Figure 8:** The variation of the load on the surface of the cement according to the quantity of NFC added

Fig. 9 depicts the amount of surfactant adsorbed as a function of starting concentration. Three zones are discernible, as follows: we can observe equilibrium in the first case at low concentration. This behavior was linked to the surface of the composite being neutralized by surfactant adsorption through electrostatic interactions.

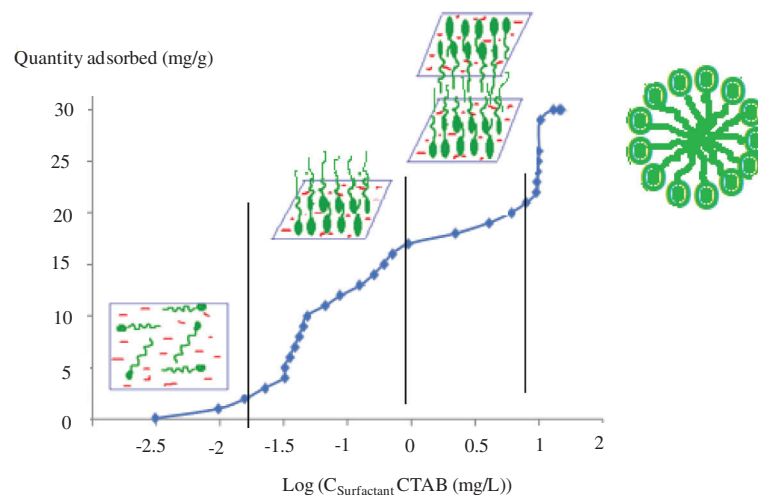


**Figure 9:** Evolution of the amount of CTAB captured by ingredient onto NFC based on the solution concentration

The intercalation of surfactant molecules with water to create the saturation of the first layer is the explanation for the slope rise in the second zone [22]. It marks the start of mineralization, and a potential of negative charge in the third zone of CTAB is observed.

Electrostatic forces in this area neutralize the surface of the mortar. At the air/water contact, hydrophobic interactions cause the surfactant molecules to be adsorbed perpendicular to the surface.

### 3.6 XRD Analysis

Fig. 10 displays the XRD spectra of both pure clay and organophilic clay. Typical reflections ( $2\Theta = 6.8^\circ$ ,  $12.1^\circ$ ,  $21.02^\circ$ ,  $26.64^\circ$ , and  $61.98^\circ$ ) are seen in the XRD diagram of pure clay. There are other peaks in the XRD pattern that represent evidence of impurities like feldspar ( $2\Theta = 27.52^\circ$ ) and quartz ( $2\Theta = 21.02^\circ$  and  $26.88^\circ$ ). After treating the clay with CTAB, there is a noticeable alteration in the diffraction pattern. The results of the organophilic clay treatment may be seen in the displacement of the primary diffraction peak from  $6.8^\circ$  to  $5.28^\circ$ . This change confirms the intercalation of the CTAB between the clay layers (Fig. 10), by the separation between the reticular planes of the family (001) which pass from  $d_{001} = 1.305 \text{ nm}$  ( $2\Theta = 6.8^\circ$ ) to  $d_{001} = 1.674 \text{ nm}$  ( $2\Theta = 5.28^\circ$ ) [33].

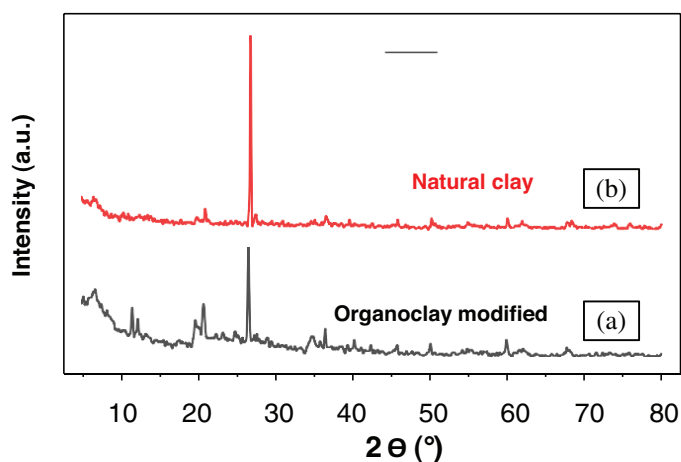


**Figure 10:** X-Ray diffraction patterns of (a) organophilic clay, (b) pure clay

### 3.7 Solid State FTIR Spectroscopy and NFC Characterization $^{13}\text{C}$ NMR

The unaltered NFC displays the recognizable bands to the cellulose skeleton at  $1456$  and  $1423 \text{ cm}^{-1}$ , respectively, corresponding to the  $-\text{OH}$  in the binding plane and the  $-\text{CH}_2-$  groups (Fig. 11). The bands of the hydrocarbon cycles, which correspond to the asymmetric vibration of  $\text{C-O-C}$ , the cycle vibration, and the  $\text{C-O}$  group, respectively, appear at roughly  $1160$ – $1110$  and  $1060$ – $1030 \text{ cm}^{-1}$  in the region between  $1200$ – $1000 \text{ cm}^{-1}$ , where the hydrocarbon cycles are frequently found. The bending of the water  $\text{OH}$  groups that are firmly linked to the surface of the fibers is what causes the peak at  $1625 \text{ cm}^{-1}$ . When  $\text{NaOH}$  was applied, the strength of the peaks at  $1732.60$  and  $1240.05 \text{ cm}^{-1}$  sharply decreased, indicating that a significant amount of hemicelluloses had been removed [28]. Two additional absorption peaks at  $1710.68 \text{ cm}^{-1}$  were visible in the IR spectra of oxidized NFC.

Fig. 12 displays the NMR spectra of the NFC and the oxidized NFC. The signals at  $104.7$ ,  $89.8$ ,  $74.7$ ,  $72$ , and  $69.5 \text{ ppm}$  in the NFC's spectrum correspond to the lengthened displacements of the glucose unit's six carbon atoms, which are represented by (C-1), (C-4), (C-5), (C-2), (C-3), and (C-6), respectively.

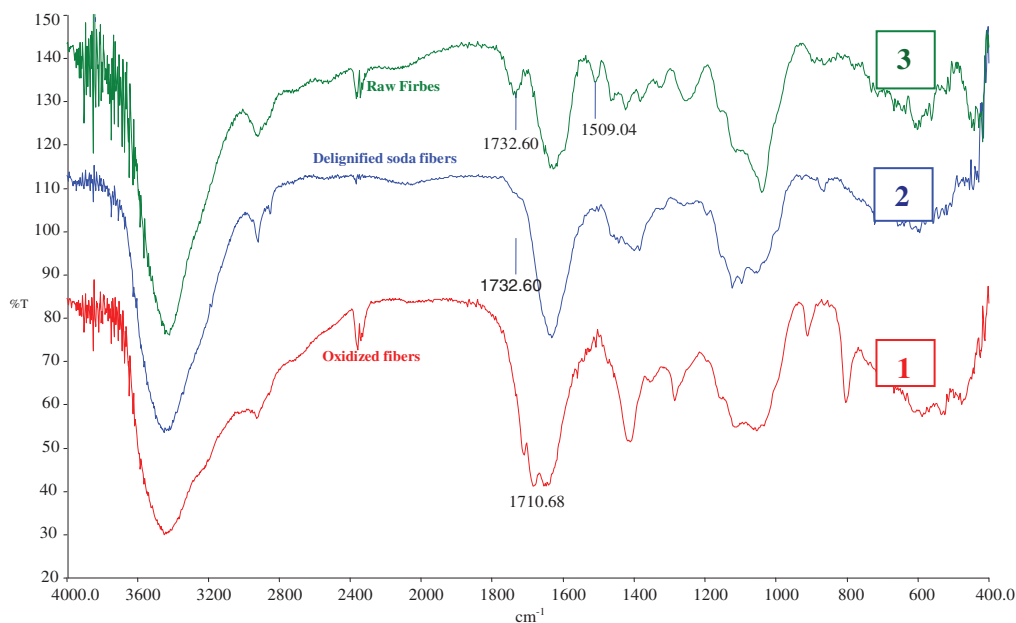


**Figure 11:** IR spectra of oxidized NFC (1), delignified soda fiber (2), and raw NFC (3)

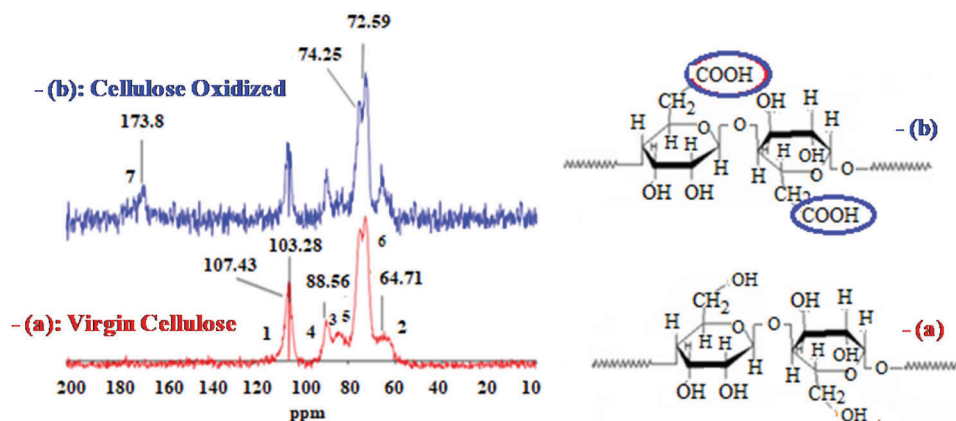


**Figure 12:**  $^{13}\text{C}$  CP-MAS solid-state NMR spectra of NFC (a), and oxidized NFC (b)

### 3.8 Identification of Organophilic-Clay by FTIR Spectroscopy

Fig. 13 presents the FTIR spectra of pure clay, clay treated with  $\text{H}_2\text{SO}_4$ , and clay modified with CTAB surfactant, showing a band around  $3624\text{--}3390\text{ cm}^{-1}$  characteristic of stretching vibration of the  $-\text{OH}$  function. The FTIR spectrum of clay treated with CTAB shows two peaks ( $2920$  and  $2851\text{ cm}^{-1}$ ) attributed to variations in the valence of the stretching vibration of the aliphatic groups  $-\text{CH}_2-$ . The band around ( $1628\text{ cm}^{-1}$ ) corresponds to the  $-\text{OH}$  bonds of water molecules adsorbed on the surface of the clay.

Fourier transform infrared spectrum reveals the presence of a stretching vibration band linked to the Si-O-Si group, peaks around  $1428$  and  $3420\text{ cm}^{-1}$  which corresponds to the stretching vibration of the  $-\text{OH}$  groups, as well as bands around  $1263$ ,  $2851$  and  $2920\text{ cm}^{-1}$ , respectively, corresponds to the stretching vibrations of  $-\text{CH}-$ . In addition, the spectrum shows a band around  $1470\text{ cm}^{-1}$  attributed to the symmetrical vibrations of the carboxylic group  $-\text{COO}^-$  of the oxidized cellulose nanofibers [34].

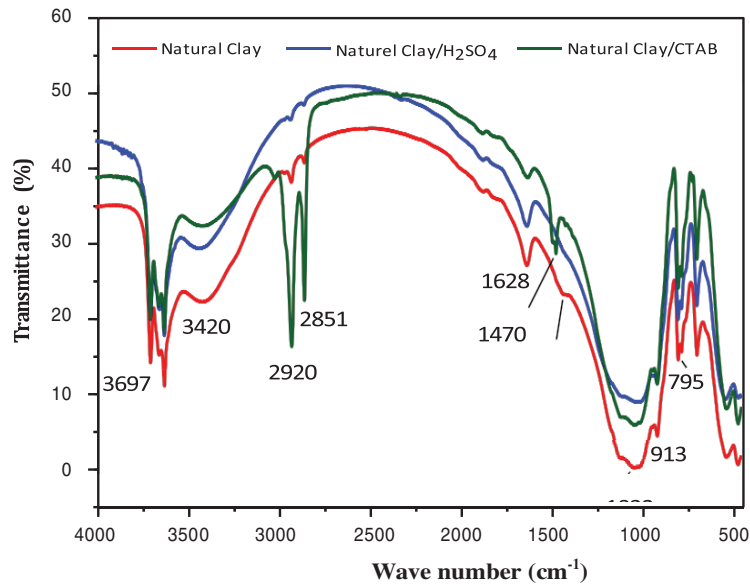


**Figure 13:** IR spectra of untreated clay and clay treated with CTAB

### 3.9 Scanning Electron Microscopy (SEM)

The surface morphology of untreated clay and clay modified by the addition of a small amount of silica gel is shown in the micrograph (Fig. 14). The plaques, each measuring 200 nm in size, are layered one on top of the other in a distinctive package resembling structure heed, as demonstrated by the image. It is easy to see that specific plates and the layers of the treated clay have successfully separated following this treatment with CTAB and its modification by the addition of silica gel.

### 3.10 Control of Density and Porosity in Cement Paste

Fig. 15 displays the density values for NFC-reinforced cement. In general, NFC containing composites are lower density than those without NFC. This may be ascribed to the void that has formed at the interface between NFC and cement matrix. Density drops by 45% for composite materials with 1.5 wt% of NFC. This shows that hemp fiber increases the density of cement composites, but NFC has a filling impact on the density of cement composites with or without NFC. The density of the cement composite was lowered by adding 1.5% weight of NFC. That enhancement showed that the addition of NFC causes the density to drop and results in a composite material with a consolidated microstructure.

The findings of cement paste, NFC reinforced composites, and NFC-OC reinforced composites porosity and water absorption values are displayed in (Fig. 15). The porosity of composites containing NFC cellulose nanofibers is often higher than that without added NFC in the composites. The creation of voids at the interface between the matrix and NFC may be responsible for this. In composites containing between 0.5 and 1 percent by weight of NFC, the porosity drops by 1.82 percent. The porosity of these composites shows that NFC has a diminishing influence on cement paste composite porosity [35,36] and that NFC concentrations of 0.5 percent weight and 1 percent weight are capable of saturating the surface and lowering pores.

Fig. 15 shows a reduction in the porosity of the composite materials produced. Indeed, 1% by weight of clay reduced the porosity of the composites by 18.75%, which explains why the organophilic clay contributed to the reduction of the porosity by saturating the voids between the cement grains. Moreover, for quantities greater than 1% by weight of organophilic clay added, the agglomeration effect led to an increase in porosity for all samples [37–39].

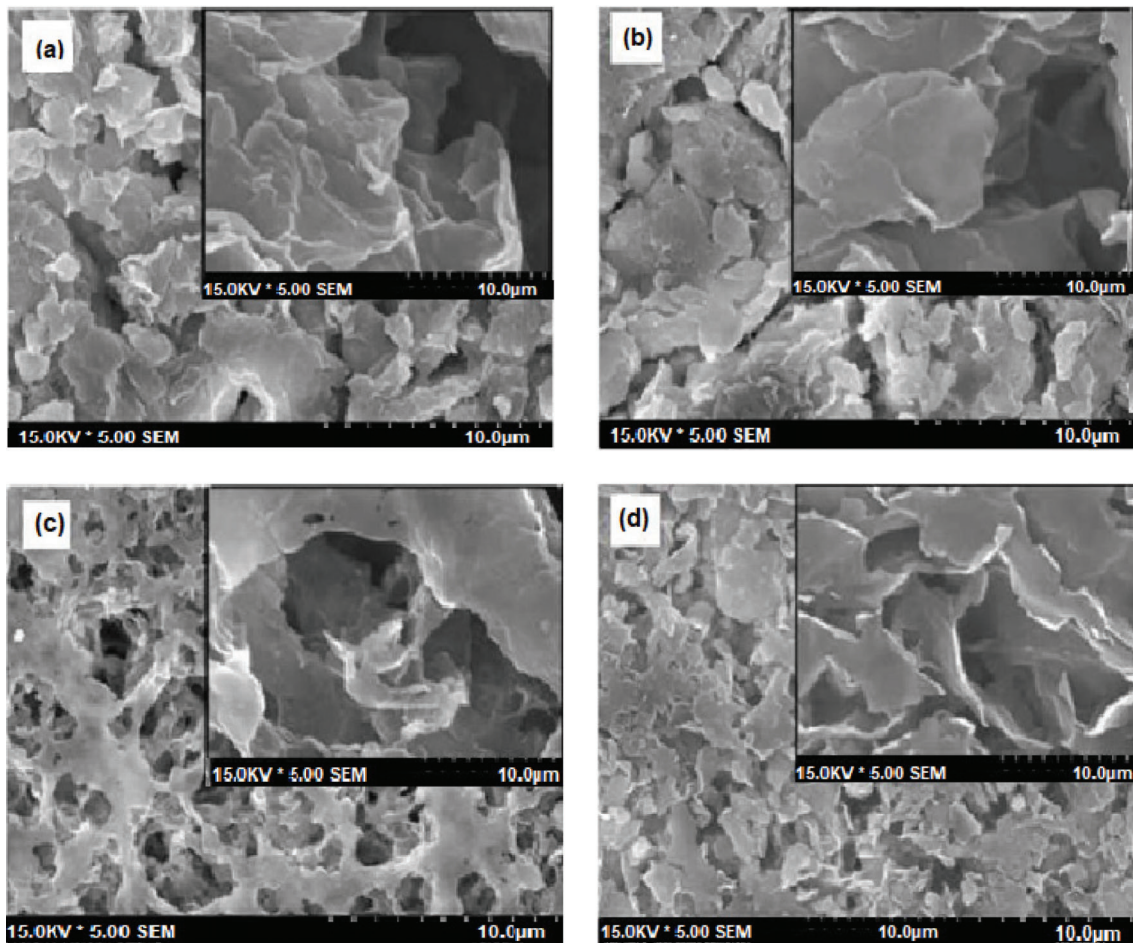


Figure 14: Scanning electron microscopy images of pure clay (a, b) and organophile clay (c, d)

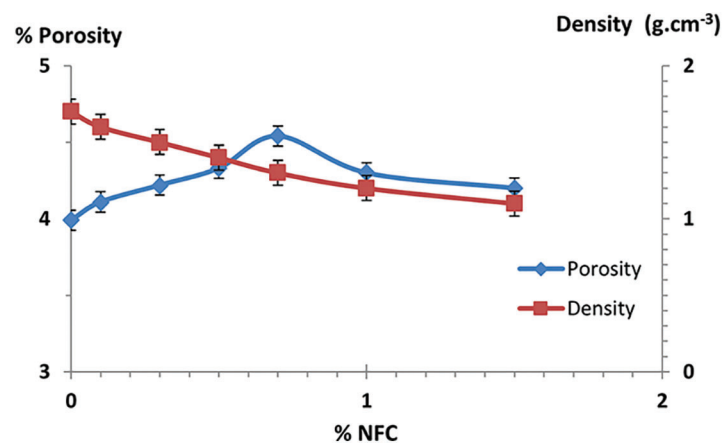
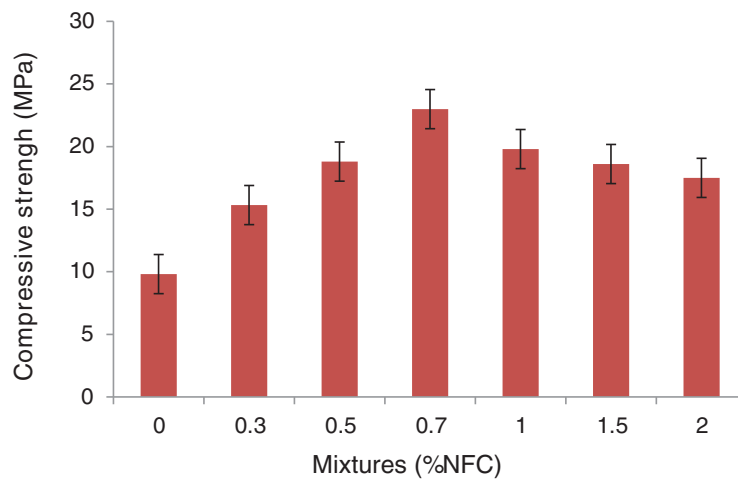


Figure 15: Porosity and density variations for control composites as a function of NFC content

### 3.11 Evaluation of Sample Mechanical Properties

The results of the studies of the mechanical properties of the cementitious composites developed, showed improvements in compressive strength by adding cellulose nanofibers [40–42]. In fact, for

cement composites reinforced with NFC treated, the compressive strength of cementitious matrix composites increased by nearly 130%, from 9.8 to 22.9 MPa (Fig. 16). The high hemicellulose content of the oxidized cellulose nanofiber can be exploited to explain the low compressive strength value. The chemical treatment, on the other hand, demonstrated high performance in mechanical properties. These factors have contributed to the improvement of the mechanical characteristics of the composites.



**Figure 16:** The cement pastes reinforced with NFC at 28 days of curing age in terms of compressive strengths

### 3.12 Thermal Conductivity

#### 3.12.1 The Impact of Fiber Count

The typical thermal conductivities of NFC-reinforced composite materials are 2.25, 1.62, 1.15, 0.95, and 1.12 W/m·K. The aforementioned findings show that increasing nanofiber concentrations of 0%, 0.3%, 0.5%, 0.7%, and 1% W/m·K each led to a 57% reduction in heat conductivity compared to the pure composite without NFC (Fig. 17). This decrease might be caused by the addition of too little NFC to encourage the formation of a homogenous framework. Additionally, the thermal conductivity of a material is influenced by several factors, including its porosity, water content, temperature, and constituent elements [43].

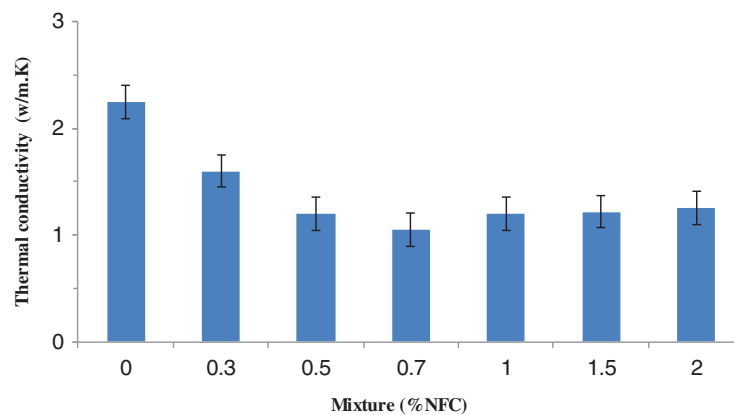


**Figure 17:** Thermal conductivity influenced by the quantity of NFC

### 3.12.2 NFC and Organophilic-Clay Impact

We looked into how thermal conductivity and porosity compared to the rate of NFC reinforcement in mortar (Fig. 17). Additionally, we observe that the porosity of this substance is increased by the addition of NFC to the cement [17,39]. Additionally, the thermal conductivity data indicated a reduction in the amount of heat propagated as the rate of CNF reinforcement in the composite material increased. The high porosity of the NFC and the significant amount of composite elements in the cement, in general, contributed to lower levels of thermal conductivity.

It may be deduced that from a rate of 0.7% by weight of NFC and 1% of organic clay, these constituents contribute to the highest thermal conductivity of the composite material compared to the reference sample. As a result, the composite heat conductivity rose as additional NFC was added, reaching a maximum of 2 wt%. The reference produced improved thermal conductivity values when compared to hybrid composites (Fig. 17). The inclusion of NFC in the composite can be used to explain these results [40]. Consequently, the NFC surface showed the presence of the new pores causing a decrease in the adhesion between the fibers and the cement matrix.

Fig. 17 shows that for reinforcement with 0.3 and 0.7 percent fibers, thermal conductivity falls as the proportion of fibers increases; this phenomenon can be attributed to the substitution of cement, an excellent natural insulator and an excellent thermal transmission. When the fiber mass reaches 1.5 percent, the thermal conductivity in this situation diminishes, the heat exchange by conduction weakens in comparison to the convective exchange, and at the same time, the proportion of pores rises. Additionally, the heat transfer of cement materials supplemented with NFC and OC varied as a function of the mass of fibers, and according to the results, it decreased as the proportion of the mass of fiber increased in comparison to the reference sample. This reduction is mainly due to the high porosity of NFC and large composite materials. It may be deduced that 0.7 wt% of NFC and the reference. OC contributes considerably to the heat conductivity of the composite materials compared to the reference sample to explain the decrease of distinct specimens. As a result, adding 1 percent weight of NFC increased the composite's heat transfer, though it was still lower than the reference. It has been discovered that the NFC surface exhibits the presence of pores, which may diminish the adherence of the fibers to the cement matrix. As a result, we can claim that the adhesion between the NFC-organophilic-clay and the matrix is crucial to the overall efficiency of the composite.

In order to highlight our results, a comparison between the values of thermal conductivity obtained in this work and those obtained in other research works is established in Table 4.

**Table 4:** Comparative table of thermal conductivity of cementitious composites

Reference	Type of reinforcement	Mass percentage added (%)	Thermal conductivity $\lambda$ (W/m·K)
Our work	NFC	0.7	0.95
[44]	Palm fibers	5	1.25
[45]	Cellulose fiber	16	1.38
[46]	Palm wood fibers	5	1.32
		30	1.21
[47]	Graphene oxide	2.5	0.88

It is very clear that we obtain almost the same values of conductivity, but the interest of our work relates to the materials of our days.

### 3.13 Blended Morphological Characteristics

Fig. 18 displays the surface morphology of specimens that were cured for seven days: Cement with 0% NFC (a) and Cement with 0.7% NFC (b). Low-volume fractions (0.7 wt%) of NFC added to the cementitious matrix make the matrix denser and less porous. These findings attest to the NFC addition's reinforcing of the cementitious matrix material and the kinetic energy of the cement hydration at the young age of curing (seven days).

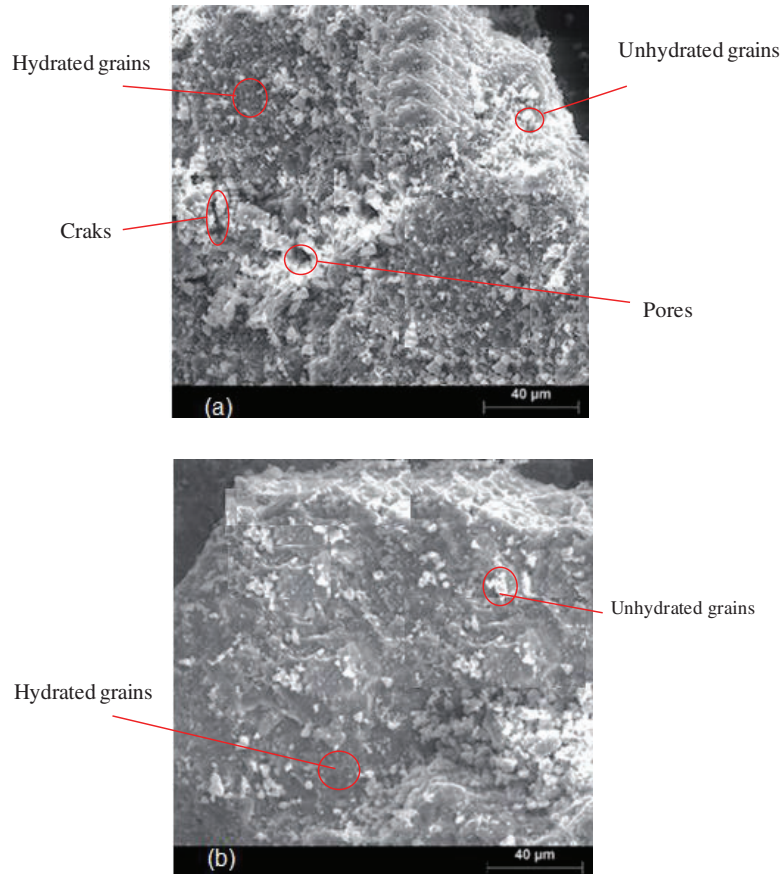


**Figure 18:** Cement with 0% NFC sample (a) and cement with 0.7% NFC sample (b) surface morphology images taken after seven days of curing

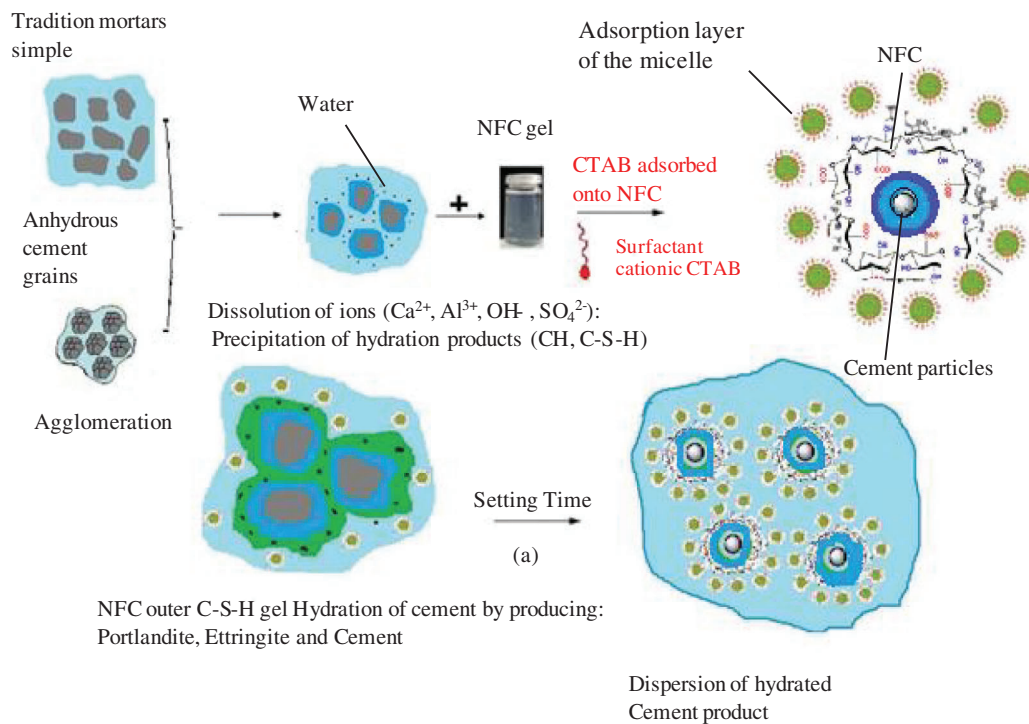
### 3.14 Effect of the Inclusion of Cellulose Nanofibers in the Presence of a CTAB Adjuvant on the Stability of the Cementitious Matrix

Fig. 19 illustrates the dispersion and stability of cellulose nanofibers by CTAB surfactants in a cementitious matrix.

- The adsorption of molecules with polar functions, such as OH,  $\text{SO}_4^-$ ,  $\text{SO}_3^{2-}$ , or  $\text{COO}^-$  type functionalities.
- In particular, it involves the binding of charged polymers as a result of the usage of super plasticizers. The interaction represents the intra-granular repulsion phenomena.
- Micelles forming at the solid-solution contact.

- d) This mechanism explains why poly-naphthalene sulphonate chemisorbs to particular reaction sites like these two aluminates.
- e) The activity of carbohydrates or hydroxyl organic acids by cross linking in the intermediate phase is suggested by this figure. The production of hydrates like portlandite or C-S-H may then be delayed as a result of this complexation.

By adhering to particular crystallographic growth sites, the CTAB surfactant may be able to prevent the formation of hydrate cement, according to the mechanism in (a). The polymer's (NFC) insertion into the hydrate structure is shown in Fig. 19.



**Figure 19:** Dispersion of NFC and state of the environment of cement grains

#### 4 Conclusions

The potential of NFC as a substrate admixture for a concrete mix was investigated in this work. Due to its hydrophilic potential, high reactivity and high specific surface area, the thermal, mechanical and microstructural properties have improved. The effects of cationic surfactant (CTAB) on the fresh and hardened properties of cementitious mortar in this study further show the heat input resulting from the use of surfactants and cellulose nanofibers (NFC) as an admixture in cementitious mortars for exterior wall insulation. New thermal insulation by a homogeneous distribution of cellulose nanofibers using an emulsion in the presence of a cationic surfactant (CTAB) in the cement mortar was prepared in this study.

The expanded organophilic-clay particles and a large number of closed pores generated effectively reduce the density and thermal conductivity of the mortar. Moreover the addition of 0.7% by weight of NFC per emulsion in the presence of a cationic surfactant (CTAB), the material produced presented its dry porosity between 4.4% and 4.7%. The compressive strength is between 9.8 and 22.9 MPa, and the thermal conductivity is between 0.95 and 2.25 W/m·K, showing better mechanical and thermal performance than traditional portland cement mortar with similar density.

Additionally, adding CTAB and NFC-treated organophilic clay to the cement matrix should result in improvements, more hydration products forming early in the curing process, and a decrease in thermal conductivity for effective insulation.

**Acknowledgement:** Authors are grateful to the Laboratory of Energy and Materials (LABEM), University of Sousse and Laboratoire Sciences des Matériaux et Environnement (LMSE), University of Sfax, Tunisia for the financial support of this work.

**Funding Statement:** The authors received no specific funding for this study.

**Conflicts of Interest:** The authors declare that they have no conflicts of interest to report regarding the present study.

## References

1. Sandberg, D., Kutnar, A., Mantanis, G. (2017). Wood modification technologies—A review. *Forest-Bio Geosciences and Forestry*, 10(6), 895–908. DOI 10.3832/for2380-010.
2. Hu, J. H., Yang, D. J. (2020). Meso-damage evolution and mechanical characteristics of low-porosity sedimentary rocks under uniaxial compression. *Transactions of Nonferrous Metals Society of China*, 30(4), 1071–1077. DOI 10.1016/S1003-6326(20)65278-5.
3. Duan, Z., Hou, S., Xiao, J., Singh, A. (2020). Rheological properties of mortar containing recycled powders from construction and demolition wastes. *Construction and Building Materials*, 237(2), 117622. DOI 10.1016/j.conbuildmat.2019.117622.
4. Zhang, J., Ma, Y. F., Wang, J., Gao, N. X., Hu, Z. L. (2022). A novel shrinkage-reducing poly carboxylate super plasticizer for cement-based materials: Synthesis, performance and mechanisms. *Construction and Building Materials*, 321(2), 126342. DOI 10.1016/j.conbuildmat.2022.126342.
5. Zhang, H. J., Zhang, X. H., Zhou, H. B. (2020). Research on acoustic emission characteristics and constitutive model of rock damage evolution with different sizes. *Advances in Civil Engineering*, 2020(16), 1–8. DOI 10.1155/2020/6660595.
6. Liu, R., Chi, Y., Chen, S., Jiang, Q., Meng, X. et al. (2020). Influence of pore structure characteristics on the mechanical and durability behavior of pervious concrete material based on image analysis. *International Journal of Concrete Structures and Materials*, 144(1), 627–642. DOI 10.1186/s40069-020-00404-1.
7. Chu, D. M., Mu, J., Avramidis, S., Rahimi, S., Liu, S. Q. et al. (2019). Functionalized surface layer on poplar wood fabricated by fire retardant and thermal densification. Part 1: Compression recovery and flammability. *Forests*, 10(11), 982–989.
8. Jesus, R. S., Barbar, M., Alo, R. B., Dag, K. D. (2019). Setting behavior and bioactivity assessment of calcium carbonate cements. *Journal of the American Ceramic Society*, 102(11), 6980–6990.
9. Schlegl, F., Gantner, J., Traunspurger, R., Albrecht, S., Leistner, P. (2019). LCA of buildings in Germany: Proposal for a future benchmark based on existing databases. *Energy Build*, 194, 342–350.
10. Pourya, M., Yasin, O., Omid, A., Masoud, S. N., Hossein, M. (2020). Green synthesis using cherry and orange juice and characterization of TbFeO<sub>3</sub> ceramic nanostructures and their application as photocatalysts under UV light for removal of organic dyes in water. *Journal of Cleaner Production*, 252, 119765.
11. Fadhel, A., Sabrine, A. (2018). Preparation and evaluation of the influence of modified fiber flour wood on the properties of the fresh condition of cement based mortars. *International Journal of Industrial Chemistry*, 9(3), 265–276. DOI 10.1007/s40090-018-0155-2.
12. Qi, X. B., Huang, Y. J., Li, X. W., Hu, Z. H., Ying, J. W. et al. (2020). Mechanical properties of sea water sea sand coral concrete modified with different cement and fiber types. *Journal of Renewable Materials*, 8(8), 915–937. DOI 10.32604/jrm.2020.010991.
13. Hassan, A., Faiz, U. A. S., Low, I. M. (2017). Effect of nanoclay on durability and mechanical properties of flax fabric reinforced geo polymer composites. *Journal of Asian Ceramic Societies*, 5(1), 62–70. DOI 10.1016/j.jascr.2017.01.003.

14. Yang, T., Wang, Z., Tan, S., Guo, F. (2020). Mechanical properties and growth mechanism of TiB<sub>2</sub>-TiC/Fe composite coating fabricated *in situ* by laser cladding. *Journal of Applied Composite Materials*, 27(1), 1–17.
15. Juliana, C. H., Styliani, P., Benjamin, N., John, M., Kevin, P. (2017). Applied clay science tailored montmorillonite nanoparticles and their behavior in the alkaline cement environment. *Applied Clay Science*, 143(6), 67–75. DOI 10.1016/j.clay.2017.03.005.
16. NT 47.05 (1983). Liants hydroliques—technique des essais-essais de retrait de gonflement. *Journal officiel de la république Tunisienne*, 70, 3178.
17. Magdalena, B., Carmen, M. P., Simon, F. C., Daniel, I. T., Graham, A. O. (2022). Effects of biological and chemical degradation on the properties of scots pine wood—Part I: Chemical composition and microstructure of the cell wall. *Materials*, 15, 2348–2362.
18. Popescu, C., Jones, D., Kržišnik, D., Humar, M. (2020). Determination of the effectiveness of a combined thermal/chemical wood modification by the use of FT-IR spectroscopy and chemometric methods. *Journal of Molecular Structure*, 1200(4), 127133–127141. DOI 10.1016/j.molstruc.2019.127133.
19. Hossam, E. S., Khaled, G. (2019). Performance of eccentrically loaded reinforced-concrete masonry columns strengthened using FRP wraps. *Journal of Composites for Construction*, 23(5), 1–12.
20. Wang, Y. L., He, F. X., Wang, J. J., Wang, C., Xiong, Z. Q. (2019). Effects of calcium bicarbonate on the properties of ordinary Portland cement paste. *Construction and Building Materials*, 225(20), 591–600. DOI 10.1016/j.conbuildmat.2019.07.262.
21. Paweł, G. K., Wiktor, W. S. (2022). Fiber-reinforced polymer composites in the construction of bridges: Opportunities, problems and challenges: A review. *Fibers*, 10(4), 37. DOI 10.3390/fib10040037.
22. Sabrine, A., Fadhel, A., David, B., Sami, B. (2007). Self-aggregation of cationic surfactants onto oxidized cellulose fibers and coadsorption of organic compounds. *Journal of Langmuir*, 23(7), 3723–3731. DOI 10.1021/la063118n.
23. Abbas, M., Lucas, B., John, V. S., Halenur, K., John, M. et al. (2019). Nanoparticles in construction materials and other applications, and implications of nanoparticle use. *Materials*, 12(19), 3052. DOI 10.3390/ma12193052.
24. Fadhel, A., Sabrine, A. (2019). Effect of modified fiber flour wood on the fresh condition properties of cement based mortars. *International Journal of Masonry Research and Innovation*, 4(4), 355–377. DOI 10.1504/IJMRI.2019.102569.
25. Fadhel, A., Sabrine, A., Habib, S. (2019). Stabilization and evaluation of modified nanofiber flours of wood on the properties of cement based mortar. *Journal of Renewable Materials*, 7(8), 763–774. DOI 10.32604/jrm.2019.04071.
26. Iskandar, B., Sabrine, A., Sami, B. (2011). Nanofibrillated cellulose from TEMPO-oxidized eucalyptus fibers: Effect of the carboxyl content. *Journal of Carbohydrate Polymer*, 84, 975–983.
27. Fadhel, A., Sabrine, A., Habib, S. (2019). Influence and dispersion of nanofiber flours of wood modified on properties of cement based mortars. *Journal of Renewable Materials*, 7(7), 631–641.
28. Low, I. M., Ahmad, H., Faiz, U. A. S. (2017). Hemp fabric reinforced organoclay–cement nanocomposites: microstructures, physical, mechanical and thermal properties. In: *High performance natural fiber-nanoclay reinforced cement nanocomposites*, 1st edition, pp. 19–36. New York: Springer. DOI 10.1007/978-3-319-56588-0\_3.
29. Ahmad, H., Faiz, U. A. S., Low, I. M. (2015). Thermal and mechanical properties of NaOH treated hemp fabric and calcined nanoclay-reinforced cement nanocomposites. *Materials & Design*, 80, 70–81.
30. Hakamy, A., Shaikh, F. U. A. (2015). Effect of calcined nanoclay on microstructural and mechanical properties of chemically treated hemp fabric-reinforced cement nanocomposites. *Construction and Building Materials*, 95, 882–891.
31. Mostafa, J., Mojtaba, F., Mohamad, F. (2013). Effects of fly ash and TiO<sub>2</sub> nanoparticles on rheological, mechanical, microstructural and thermal properties of high strength self-compacting concrete. *Journal of Mechanics of Materials*, 61, 11–27.

32. Gihan, G., Alaa, M. S., Emad, S. H. B. (2021). Application of nano waste particles in concrete for sustainable construction: A comparative study. *International Journal of Sustainable Engineering*, 14(6), 2041–2047. DOI 10.1080/19397038.2021.1963004.
33. Jinfeng, S., Hu, S., Binbin, Q., Zhiqing, X. (2017). Effects of synthetic C-S-H/PCE nanocomposites on early cement hydration. *Construction and Building Materials*, 140(10), 282–292. DOI 10.1016/j.conbuildmat.2017.02.075.
34. Katarzyna, S., Katarzyna, N., Monika, M., Kai, B. (2015). Preliminary selection of clay minerals for the removal of pharmaceuticals, bisphenol A and triclosan in acidic and neutral aqueous solutions. *Journal of Comptes Rendus Chimie*, 18(10), 1134–1142.
35. Tang, Z., Li, W., Lin, X., Xiao, H., Miao, Q. et al. (2017). TEMPO-oxidized cellulose with high degree of oxidation. *Polymers*, 9(9), 421. DOI 10.3390/polym9090421.
36. Marta, R. F., Pedro, S. (2020). Concrete early-age crack closing by autogenous healing. *Sustainability*, 12(11), 4476–4492. DOI 10.3390/su12114476.
37. Wiesława, N. W., Katarzyna, S. (2019). Calorimetry in the studies of by-pass cement kiln dust as an additive to the calcium aluminate cement. *Journal of Thermal Analysis and Calorimetry*, 138(6), 4561–4569. DOI 10.1007/s10973-019-08913-2.
38. Norhasri, M. S. M., Hamidah, M. S., Fadzil, A. M. (2017). Applications of using nano-material in concrete: A review. *Construction and Building Materials*, 133(4), 91–97. DOI 10.1016/j.conbuildmat.2016.12.005.
39. Seydibeyoğlu, M.Ö., Oksman, K. (2008). Novel nanocomposites based on polyurethane and micro fibrillated cellulose. *Composites Science and Technology*, 68(3–4), 908–909. DOI 10.1016/j.compscitech.2007.08.008.
40. Shimazaki, Y., Miyazaki, Y., Takezawa, Y., Nogi, M., Abe, K. (2007). Excellent thermal conductivity of transparent cellulose nanofiber/epoxy resin nanocomposites. *Journal of Biomacromolecules*, 8(9), 2976–2978. DOI 10.1021/bm7004998.
41. Antonio, N. N., Hiroyuki, Y. (2008). The effect of fiber content on the mechanical and thermal expansion properties of bio composites based on microfibrillated cellulose. *Journal of Cellulose*, 15(4), 555–559. DOI 10.1007/s10570-008-9212-x.
42. Onuaguluchi, O., Panesar, D. K., Sain, M. (2014). Properties of nanofibre reinforced cement composites. *Construction and Building Materials*, 63(6), 119–124. DOI 10.1016/j.conbuildmat.2014.04.072.
43. Cao, Y., Zavaterri, P., Youngblood, J., Moon, R., Weiss, J. (2015). The influence of cellulose nanocrystal additions on the performance of cement paste. *Cement Concrete Composite*, 56(7), 73–83. DOI 10.1016/j.cemconcomp.2014.11.008.
44. ArdanuyRaso, M., Claramunt Blanes, J., Parés Sabatés, F., Aracri, E., Vidal Lluciá, T. (2012). Nanofibrillated cellulose (NFC) as a potential reinforcement for high performance cement mortar. *Journal of Composites*, 7, 3883–3894.
45. Ma, L., Guo, C., Ou, R., Sun, L., Wang, Q. et al. (2018). Preparation and characterization of modified porous wood flour/lauric-myristic acid eutectic mixture as a form-stable phase change material. *Energy and Fuels*, 32(4), 5453–5461. DOI 10.1021/acs.energyfuels.7b03933.
46. Hisseine, O. A., Wilson, W., Sorelli, L., Tolnai, B., Tagnit-Hamou, A. (2019). Nanocellulose for improved concrete performance: A macro-to-micro investigation for disclosing the effects of cellulose filaments on strength of cement systems. *Construction and Building Materials*, 206(11), 84–96. DOI 10.1016/j.conbuildmat.2019.02.042.
47. Li, X., Liu, Z., Lv, Y., Cai, L., Jiang, W. et al. (2019). Influence of graphene oxide on hydration characteristics of tricalcium silicate. *Advances in Cement Research*, 31(10), 448–456. DOI 10.1680/jadcr.17.00191.